Embedded 3D printing of dilute particle suspensions into dense complex tissue fibers using shear thinning xanthan baths

Trikalitis, Vasileios D.; Kroese, Niels J.J.; Kaya, Mert; Cofiño-Fabres, Carla; Ten Den, Simone; Khalil, Islam S.M.; Misra, Sarthak; Koopman, Bart F.J.M.; Passier, Robert; Schwach, Verena

Published in:
Biofabrication

DOI:
10.1088/1758-5090/aca124

Biofabrication

PAPER

Embedded 3D printing of dilute particle suspensions into dense complex tissue fibers using shear thinning xanthan baths

Vasileios D Trikalitis[1], Niels J J Kroese[2], Mert Kaya[3,4], Carla Cofiño-Fabres[2], Simone ten Den[2], Islam S M Khalil[3], Sarthak Misra[3,4], Bart F J M Koopman[1], Robert Passier[2], Verena Schwach[2] and Jeroen Rouwkema[1,*]

[1] Department of Biomechanical Engineering, Vascularization Lab, University of Twente, Technical Medical Centre, 7500AE Enschede, The Netherlands
[2] Department of Applied Stem Cell Technologies, University of Twente, Technical Medical Centre, 7500AE Enschede, The Netherlands
[3] Surgical Robotics Laboratory, Department of Biomechanical Engineering, University of Twente, TechMed Center, MESA+ Institute, 7500AE Enschede, The Netherlands
[4] Surgical Robotics Laboratory, Department of Biomedical Engineering, University of Groningen and University Medical Centre Groningen, 9713AV Groningen, The Netherlands
* Author to whom any correspondence should be addressed.

E-mail: j.rouwkema@utwente.nl

Keywords: 3D bioprinting, tissue, particles

Supplementary material for this article is available online

OPEN ACCESS

RECEIVED
7 August 2022

REVISED
24 October 2022

ACCEPTED FOR PUBLICATION
8 November 2022

PUBLISHED
6 December 2022

Abstract

In order to fabricate functional organoids and microtissues, a high cell density is generally required. As such, the placement of cell suspensions in molds or microwells to allow for cell concentration by sedimentation is the current standard for the production of organoids and microtissues. Even though molds offer some level of control over the shape of the resulting microtissue, this control is limited as microtissues tend to compact towards a sphere after sedimentation of the cells. 3D bioprinting on the other hand offers complete control over the shape of the resulting structure. Even though the printing of dense cell suspensions in the ink has been reported, extruding dense cellular suspensions is challenging and generally results in high shear stresses on the cells and a poor shape fidelity of the print. As such, additional materials such as hydrogels are added in the bioink to limit shear stresses, and to improve shape fidelity and resolution. The maximum cell concentration that can be incorporated in a hydrogel-based ink before the ink's rheological properties are compromised, is significantly lower than the concentration in a tissue equivalent. Additionally, the hydrogel components often interfere with cellular self-assembly processes. To circumvent these limitations, we report a simple and inexpensive xanthan bath based embedded printing method to 3D print dense functional linear tissues using dilute particle suspensions consisting of cells, spheroids, hydrogel beads, or combinations thereof. Using this method, we demonstrated the self-organization of functional cardiac tissue fibers with a layer of epicardial cells surrounding a body of cardiomyocytes.

1. Introduction

Three-dimensional (3D) bioprinting, a branch of additive manufacturing, is increasingly used in the field of tissue engineering to assemble structures that resemble the composition, architecture and function of biological tissue [1, 2]. The goal is to create engineered tissue constructs, which consist of intricate architectures of multiple cell types and their extracellular matrix. In nature, comparable tissues are the result of complex self-assembly processes, for instance during embryonic development [3]. While it has not been yet possible to fully replicate this process, advances in bioprinted microtissues can be utilized to study and gain insights in the development of these tissues and organs through organoid assembly [4], understand disease mechanisms better, screen and test pharmaceutical formulations [4], or use them as an implant to repair damage in an existing organ or tissue [5]. Tissue engineering strategies can be divided into two broad categories: scaffold based, where materials and cells are

combined into a composite, and scaffold-free, where only cellular matter, such as cells or spheroids, is used for tissue fabrication [6]. The overwhelming majority of extrusion 3D bioprinting can be considered as scaffold based [7], since biomaterial based bioinks are employed, to fulfill the necessary rheological prerequisites of shear thinning and shear recovery, in order to achieve deposition and shape fidelity of a construct [8, 9]. Whether it is a hydrogel that has been tailored to mimic the extracellular matrix (ECM) of cells [10], or actual ECM being incorporated into the ink phase [11], the added material will affect both the rheological and biological behavior of the bioink and the cellular content.

Organoid research has shown us that cells can assemble into complex, physiological tissue structures in a scaffold-free setting when high cell densities are used [12, 13]. Scaffold-free or cell-only extrusion 3D bioprinting, in the few instances it has been demonstrated [14–17], also shows consistently self-assembly into dense tissue constructs. However, shear stress arising from the extrusion of tightly packed cells is a crucial parameter that limits the extrudability of these material-free inks. It has been shown that high concentration cell-only inks display high viscosity values, up to a factor 1.000 higher compared to the cell-free liquid for a cell volume fraction of 60% [18]. Relatively high pressures are needed for extrusion of these suspensions, which negatively impacts cell viability [19, 20]. Additionally, cells are not shielded from the high shear stresses by additional hydrogel material. High shear stress values can be lethal for most cells, and especially for stem cells, shear stress acts as a potentially unwanted differentiation cue [21, 22]. To limit shear stresses on cells during extrusion, it would therefore be beneficial to use low viscosity bioinks with a low concentration of cells. However, these inks do not result in the high cell densities that are needed for cellular self-assembly within the printed construct.

With seminal works demonstrating embedded printing in bulk fluids [23] and in granular media [24], a paradigm shift was triggered in 3D bioprinting [25], as it allowed the 3D printing of low viscosity bioinks that do not retain their fidelity in fused deposition modeling (FDM) conditions [24, 26]. Popular variations of the granular embedding baths, like Freeform Reversible Embedding of Suspended Hydrogels (FRESH) [25], allowed the extraction of the printed structures by triggering a thermal collapse of gelatin microparticles. In another variation named Sacrificial Writing into Functional Tissue (SWIFT) [27], the granular embedding bath consisted of cell spheroids, and sacrificial channels were printed within them forming perfusable tissue blocks. Notably, the printing of high concentration cell only suspensions was demonstrated in a carbomere granular bath, showing very high fidelity and shape control [15].

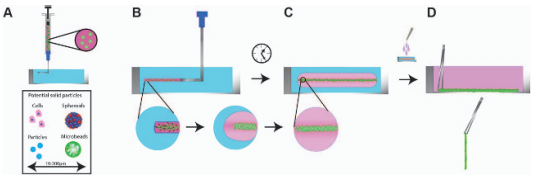

Figure 1. Graphical abstract. (A) Dilute $\varphi_p < 0.1$ particles in liquid suspension inks are loaded in a syringe with a 90° bent needle. (B) The suspension inks are printed within a xanthan gum (XG) embedding bath forming linear aqueous viscosity features. (C) After printing, the liquid phase of the suspension diffuses radially into the embedding bath, which allows the assembly of dense particle structures. In the case of cellular matter, after packing, fusion into tissue structure occurs. (D) After incubation, the xanthan embedding bath can be diluted to aqueous viscosities through the addition of water, or cell medium in the case of cellular matter, and those structures can be extracted.

Xanthan gum (XG) is a polysaccharide of bacterial origin. It is a highly utilized and inexpensive material in for instance the food industry, where it is generally used as a thickening agent. XG has also been recognized as a promising agent for tissue engineering applications due its good biocompatibility, biodegradability, cytocompatibility, high viscosity and shear thinning properties [28]. XG has been used in embedding matrices as a dispersant additive in a granular medium, or on its own as a shear thinning pseudoplastic yield stress fluid matrix [29, 30].

Even though reported embedded printing approaches have clearly demonstrated the potential of this technology, the majority of publications either use inks with a very high cell density resulting in the exposure of the cells to high shear stress values, or they result in printed constructs with a low cell density which can impede self-assembly into dense tissue structures. In the few cases of embedded printing of cell-only inks, either the surrounding embedding bath negatively affects cell viability [15], or the cells mix and interact with the surrounding environment [14, 16]. In the only reported case by Brassard *et al* where high cell viability is reported and extrusion of cell suspensions resulted in self-assembly, a complex embedding bath recipe and custom extrusion equipment were needed. Additionally, even though the presented data suggests that the cells are packed after printing, this process is not described [17].

In this paper, we present an approach of bioprinting dilute aqueous suspensions into dense microtissues. Similar to the work of Nelson *et al* [31] we are printing droplets and lines within a yield stress fluid bath, with the key adaptation that the suspension used in this study consists of a liquid that is miscible with the embedding bath. Furthermore, the bioinks portray the viscosity of an aqueous solution, thus minimizing the pressures that are needed for extrusion and the shear stresses developed within the ink. Inks are printed in a xanthan embedding bath

(figure 1(B)), after which liquid diffuses radially out from the printed structure (figure 1(C)). This results in a drastic liquid volume fraction reduction of the suspension, thus concentrating the particles at the location of the plotted trajectory. We demonstrate that this leads to the self-assembly of a complex microtissue fiber, consisting only of the particle fraction of the bioink (figures 1(C) and (D)). Additionally we show that this approach is compatible with multiple spherical entities, including cells, cell spheroids, and hydrogel microbeads, which offer the potential to include controlled chemical or mechanical stimulation of the developing tissue [32].

2. Methods

2.1. Cell culture

Human pluripotent stem cells (hPSCs) (Coriell, GM25256); double reporter human embryonic stem cell (hESC) line (HES3) mRubyII-ACTN2 and green fluorescent protein (GFP)-NKX2.5 (DRRAGN [41]); double reporter hESC line (HES3) NKX2.5eGFP/+−chick ovalbumin upstream promoter transcription factor (COUP-TFII$^{mCherry/+}$) [33] were cultured in Essential 8 medium (ThermoFisher, 1517001) on vitronectin-coated (ThermoFisher, A14700) plates and were passaged twice a week using EDTA (ThermoFisher, 15575020). Double Reporter mRubyII-ACTN2 and GFP-NKX2.5 (DRRAGN) hPSCs were differentiated to cardiomyocytes (CMs) using growth factor-based differentiation as described previously [34]. At day 14 of differentiation, cells were purified using 5 mM of lactate-containing CM-TDI medium (containing triiodothyronine, dexamethasone, and insulin-like growth factor-1) for 3 d before cryopreservation.

For epicardial differentiation [35], NKX2.5$^{eGFP/+}$ eGFP/+−COUP-TFII$^{mCherry/+}$ reporter hPSCs, were seeded on growth factor reduced (GFR) Matrigel-coated plates (Corning, 354230) at a density of 20×10^3 cm^{-2} the day before differentiation. The day after, cardiac mesoderm was induced by 20 ng ml^{-1} bone morphogenetic protein 4 (BMP4) (R&D Systems, 314-BP/CF), 20 ng ml^{-1} ACTIVIN A (Miltenyi Biotec, 130-115-010) and 1.5 μM GSK3 inhibitor and Wnt activator CHIR99021 (Axon Medchem, CT 99021). After 3 d, cytokines were removed and the Wingless/Integration-1 (WNT) inhibitor XAV939 (R&D Systems, 3748) (5 μM) was added for 3 d together with retinoic acid (RA; Sigma-Aldrich, R2625) (1 μM) and BMP4 (30 ng ml^{-1}) in BPEL medium. At day 6, RA (1 μM), and BMP4 (30 ng ml^{-1}) were refreshed. At day 9, (25×103 cm^2) cells were seeded on plates coated with 5 μg ml^{-1} of fibronectin (Sigma-Aldrich, F1141) in BPEL-medium supplemented with 10 μM of the transforming growth factor (TGF)β-inhibitor SB431542 (Sigma-Aldrich, F1141) (ECC-medium). HPSC-derived epicardial cells were confluent and ready for cryopreservation after about 4 d.

For experiments where the bioink consisted of a mix of separate cells and particles, thawed passage (P) 4 red fluorescent protein (RFP)-expressing human aortic smooth muscle cells (SMCs; Angio-Proteomie, cAP-0026RFP) were seeded at 2.7×10^3 cm^{-2} in SMC growth medium-2 + supplements (Lonza, CC-3182 + CC-4149) + 1% P/S (SMC-GM2). During culture, medium was changed every 2 d. Using TrypLE (1X) they were dissociated at day 7, reseeded at 9.5×10^3 cm^{-2} and cultured further in SMC-GM1: 76.5% Dulbecco's Modified Eagle's Medium (DMEM) (ThermoFisher, 41965-039)), 20% fetal bovine serum (Sigma Aldrich, F7524), 2.5% 1M 4-(2-hydroxyethyl)-1-piperazineethanesulfonic acid (HEPES) (Fisher Scientific, BP310) in phosphate-buffered saline (PBS; ThermoFisher, 18912-014) and 1% P/S. At day 15 they were dissociated for bioink preparations.

For the print where particles and SMC spheroids were combined, SMCs were reseeded into 4% agarose (Invitrogen, 16500) molds consisting of cylindrical microwells, having a diameter and depth of 200 μm, at ±267 cells/μwell.

After a 7 day culture, during which half the medium was changed daily with SMC-GM2 and an average spheroid diameter of 67 μm was reached, they were flushed out and collected for bioink preparations.

For the SMC-spheroids only bioink, the SMC culture, subsequent spheroid formation and collection was the same as mentioned prior, except SMC-GM2 (Cell Applications, 311) with 1% P/S (SMC-GM3) was used as a medium and the average diameter was 112 μm.

2.2. Bioink preparation

2.2.1. SMC Col-poly(lactic acid) (PLA) suspension inks

SMCs were centrifuged at 230 $*g$ for 3 min and resuspended in SMC-GM2 to be used directly in the bioink. Suspended collagen coated PLA microparticles with a diameter of 30 μm, (Micromod, 11-25-304) were centrifuged at 200 $*g$ for 1 min. After aspirating the supernatant, they were resuspended in 1000 U ml^{-1} penicillin, and 100 mg ml^{-1} streptomycin in PBS and incubated at 37 °C for 4 h, after which they were centrifuged at 200 $*g$ for 1 min (Eppendorf, 5810R) and resuspended in SMC-GM2.

The ink consisted of 0.074 φ_p SMCs (7.6 M ml^{-1}), 0.013 φ_p Col-PLA particles, 24% OptiPrep (STEMCELL Technologies, 07820) in 67% SMC-GM2.

2.2.2. SMC spheroids and Col-PLA suspension inks

SMC-spheroids and Col-PLA particles were combined in a bioink by resuspending them with SMC-spheroids, centrifuged at 960 $^*g$ for 1 min. The final ink consisted of 0.017 φ_p SMC-spheroids and

0.017 φ_p particles in 46% OptiPrep and 51% SMC-GM2.

2.2.3. SMCs spheroid inks
For prints where only SMC-spheroids were printed, spheroids were resuspended in 70% SMC-GM1 and 20% OptiPrep at 0.1 φ_p.

2.2.4. PLA particle inks
Plain 30 μm PLA particles (Micromod, 11-00-203) were disinfected in the same manner as the Col-PLA particles. After which they were resuspended in 80% OptiPrep + 10% P/S creating a 0.1 φ_p ink.

2.2.5. CMs/ECCs inks
ECCs made from hPSCs and 3A1 derived CMs were thawed and resuspended in DMEM, centrifuged at 240 $*g$ for 5 min and resuspended at 0.05 φ_p epicardial cell (ECCs) (27.2 M ml^{-1}) and 0.05 φ_p CMs (12.1 M ml^{-1}) in 70% CM-TDI and 10% OptiPrep for a 0.1 φ_p ink.

2.2.6. CM inks
DRRAGN line derived CMs were thawed and centrifuged at 240 $*g$ for 3 min. They were then resuspended at 15.3 M ml^{-1} in CM-Med1 supplemented with 20% OptiPrep, 3.9 μg ml^{-1} human collagen type I (hCol-I; Merck, CC050) and 5.8 μg ml^{-1} human collagen type III (hCol-III; Merck, CC054) for a bioink with 0.063 φ_p.

2.2.7. IPCSs inks
Dissociated WTC hiPSCs (GM25256) cultured on E8 were centrifuged at 230 $*g$ for 3 min and resuspended in 70% E8 and 20% OptiPrep, to a concentration of 41.8 M ml^{-1} creating a 0.134 φ_p bioink.

2.2.8. Hydrogel particle inks
Suspended fluorescein (FITC) labeled alginate hydrogel microbeads (average diameter $\pm$160 μm) were prepared using in-air microfluidics as described here [36]. A 0.1 φ_p ink of hydrogel beads in a 12% OptiPrep solution was prepared and 3D printed.

2.3. Preparations of embedding baths
The embedding baths were prepared by mixing XG powder (Sigma-Aldrich, SLCF8454) with cell-specific culture medium in a 50 ml centrifuge tube, shaken vigorously, and put on a roller shaker overnight at room temperature (RT), during which a homogenous hydrogel formed. For Newtonian fluid embedding baths, 1.5% XG and 1.5% sodium alginate (SA; Wako, 196-13325) powders were mixed in a 1:1 ratio prior to adding medium. Before use, the hydrogel was centrifuged at 200 $*g$ for 2 min to remove air bubbles. Hydrogels made from Dulbecco's phosphate-buffered saline (DPBS) and DMEM showed less viscous characteristics which allowed easier degassing through vacuum. $\pm$7 ml of XG was added to a 35 mm NTCT Petri dish (Greiner bio-one, 627161) creating a bath $\pm$7 mm in height. The dish was then stored in a 37 °C incubator for 3 and 4 h before printing.

2.4. 3D bioprinting
The bioinks were loaded into a 1 ml syringe (BD, 309628) using a 1000 μl pipette tip. A blunt 90° bent stainless steel G23 (406 μm inner diameter (ID), 635 μm outer diameter (OD)), G27 (229 μm ID, 406 μm OD) or G30 (152 μm ID, 305 μm OD) needle (NeedlEZ) was fitted for printing CMs/ECCs, SMC-Spheroids, SMC-Spheroids and Col-PLA-particles, SMCs and Col-PLA-particles, PLA-particles and alginate hydrogel particles. A straight G22 blunt tip needle (410 μm ID, 720 μm OD, CELLINK) was used when printing in a XG/alginate bath or XG hydrogel bioink.

The syringe was then installed into a ROKIT INVIVO hybrid 3D printer (ROKIT Healthcare). The nozzles were lowered into the 37 °C embedding bath's dish to $\pm$3 mm above its bottom. While the nozzle was static, the printbed was moved 3 mm towards the needle tip direction at 3 mm s^{-1} followed by 10 mm movement at 2 mm s^{-1} during which bioink was extruded at a constant feed rate. The printer then slowed to 1 mm s^{-1} for 2 mm after which movement and extrusion was paused for $\pm$2 min before nozzle removal, in order to not create major bath disturbances during the most critical period of the diffusion packing effect. During the printing session, syringes with bioinks containing PLA-μPs, with densities significantly higher than those of cells, were carefully shaken every 3 and 4 min for homogenization.

2.5. Post print culture
After printing, the constructs were cultured in the same dish for up to the duration of the experiment at 37 °C, 20% O_2 and 5% CO_2. The supporting bath was diluted by carefully aspiring 1.5–2 ml of hydrogel medium and replacing this volume with cell-specific medium or media every 1–3 d. In case of: (a) CMs: CM-Med1, (b) CMs/ECCs constructs: a 1:1 mix between CM-Med1 and ECC-medium, (c) iPSCs: E8 + 0.5% RevitaCell, (d) SMC (-spheroids) and Col-PLA-particles: SMC-GM2 and (e) SMC-spheroids only: SMC-GM3. Tissue constructs that self-assembled over time, could be extracted after sufficient dilution of the bath, via liquid addition on top of the bath.

2.6. Imaging of 3D printing
Fluorescent particles for multicolor microscopy were fabricated by grinding fibers synthesized using electrospinning. Polymer solution for electrospinning was prepared by dissolving polystyrene (PS) pellets (430102-1KG, Sigma-Aldrich, USA) in anhydrous N, N-dimethylformamide (DMF) (227056-1L, Sigma-Aldrich, USA). Coumarin 6 (442631-1G,

Sigma-Aldrich, USA) was selected to make the polymer solution fluorescent since it is stable in PS matrix and has relatively high photobleaching resistance. For beaded fiber synthesis, 30.0% (29.8% PS and 0.2% coumarin (6) weight-to-volume ratio in DMF was prepared and homogenized overnight at RT using a tilt-and-roll mixer (LLG-uniRoller 6, LLG-Labware, Germany). The electrospinning process was performed with an acceleration voltage of 14 kV, solution feed rate of 2.5 ml h^{-1}, and needle (18-gauge) tip-to-collector distance of 16 cm [37]. Randomly oriented fibers were deposited on a grounded aluminum foil at 24 °C and relative humidity of 22%. The deposited fiber meshes were cut into 2 and 3 mm pieces using a scalpel and transferred into a glass vial containing 1% (volume/volume) Tween 80 (P4780-100ML, Sigma-Aldrich, USA) in Milli-Q water. The grinding process, which mechanically breaks the continuous fibers using ultrasound waves, was performed using a sonicator (2510, Branson, USA) for 2 h to obtain fluorescent particles ranging in size from 5 μm to 65 μm. Real-time widefield fluorescence microscopy was performed to visualize the 3D printing of fibers using the particles inside the xanthan embedding bath (figure 3(A)). In order to render XG visible by fluorescence imaging, it was stained with fluorescein sodium (F6377-100G, Sigma-Aldrich, USA). Fabricated particles stained with coumarin 6 were placed in rhodamine B (K94900-25, Labshop, the Netherlands) labeled Milli-Q water. Coumarin 6 and fluorescein sodium have overlapping excitation and emission spectra (figure 3(C)). The concentration of fluorescein sodium in the xanthan was adjusted to be five times less than the brightness of the particles in the acquired fluorescence images. The difference in intensity levels enables the separation of the xanthan regions and the particles using a predefined thresholding value. The 10× and 2× long-working distance apochromatic objective lenses (Plan Apo, Mitutoyo, Japan) were employed to focus the excitation light to the nozzle tip in the xanthan bath and collect emitted fluorescent light for image formation, respectively [38]. Upon the thresholding, images containing Milli-Q water, particles, and xanthan were encoded with red-black, green-black, and blue-black color maps, respectively. Multicolor visualization of the 3D printing was acquired by overlaying the color-coded images (figure 3(D)).

2.7. Imaging of tissues

Images were taken using an EVOS FL AUTO 2 (ThermoFisher Scientific), an EVOS FL (ThermoFisher Scientific), A Zeiss LSM800 confocal microscope, and a Nikon ECLIPSE Ti2 (Nikon Instruments) after which they were analyzed using ImageJ/Fiji.

2.8. Tissue electrical stimulation

A 10 ms biphasic electrical potential pulse of 20 V cm^{-1} was established over the length of CMs/ECCs tissue, shown in figures 5(B)–(E) floating in 1:1 CM-Med1:ECC-med at day 14 after printing, creating a different frequency of contraction compared to its spontaneous rhythm. Pulsation of 1.0, 1.5, 2.0, 2.5, 3.0, 3.5, 4.0 Hz was performed in sequence, with 2 min pauses in-between. Videos were obtained using the Nikon ECLIPSE Ti2 over a 10 s period. Due to the elongated shape of the tissue (3750 μm × 200 μm) the contraction was most pronounced along its main axis. In each frame, certain pixels on its tips were tracked. The separation between these points was plotted as relative displacement (figures 5(E) and (F)).

2.9. Immunofluorescence analysis

The 3D-bioprinted SMC spheroid-particle composites were whole-mount stained. Fixation with 4% paraformaldehyde was carried for 1 h at RT. Afterwards, constructs were washed at RT with 0.3% Triton-X 100 (Sigma-Aldrich; 3 × 20 min) and blocked for non-specific binding with 5% BSA, 0.3% Triton-X 100, and 0.1% Tween in PBS overnight at 4 °C. Primary antibodies rabbit anti-human SM22 (Abcam, cat n. ab14106) and mouse anti-human ZO-1 (BDbiosciences, cat n. 610967) in 1:200 dilution were added for 2 d at 4 °C. Tissues were washed at RT with 0.3% Triton-X 100 (3 × 20 min). Secondary antibodies Goat anti Rabbit IgG Alexa Fluor 647 (Thermo Fisher Scientific, cat n. A21244), Goat anti Mouse IgG Alexa Fluor 488 (Invitrogen, cat n. R37120) and DAPI were added overnight at 4 °C and protected from light. Next day, tissues were washed three times with PBS for 20 min each at RT. Confocal imaging was performed with a Zeiss LSM 880 microscope.

3. Results

3.1. Optimization of printing parameters

In order to achieve consistent ink behavior and to allow for relevant printing times, a density modifier (Iodixanol) was included in the ink to maintain a homogeneous distribution of the suspension (figure 2(A (i–iii))). Failing to match the density of the particles with the liquid fraction of the ink resulted either in clogging of the nozzle due to sedimentation in the case where the density of particles is higher than the density of the surrounding liquid, or in inconsistent printing if the particles moved to the top of the cartridge in the case where the density of particles is lower than the density of the surrounding liquid. Without density matching, the operational window was limited to approximately 10 min after ink preparation when incorporating hydrogel particles and cells. From a physics perspective, cells, spheroids, and hydrogel beads are water-containing spherical particles with a finite border. When homogenously dispersed in a density-matched liquid phase at a low particle volume fraction ($\varphi_p < 0.1$), the particles do not feel each other's locally perturbed

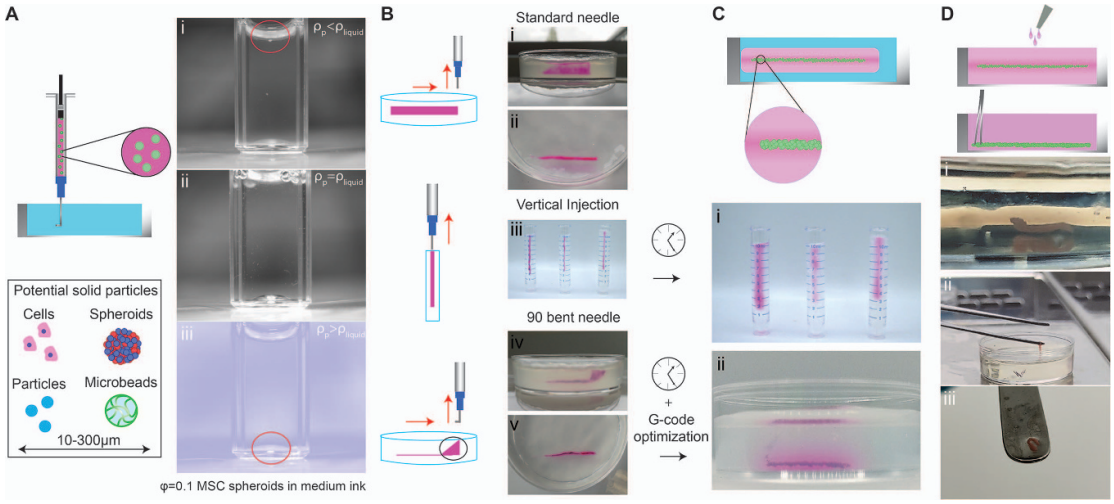

Figure 2. Embedded 3D printing of Newtonian fluids and dilute suspensions. (A) Particle suspensions, with matched, and mismatched density after centrifuging for 15 min 240 $*g$. Matching the density of particles with the medium extends the operational window of the suspension inks since sedimentation or floatation is prevented, while it simultaneously ensures homogenous dispersity of the particles over the liquid phase. (B) Effect of printing direction. Printing Newtonian fluids in a 1.5% w/v xanthan bath, results in a backflow of the liquid across the direction of the needle. Printing vertically allows the formation of columns, and using a 90° bent nozzle allows the printing of horizontal features. (C) Demonstration of diffusion of liquid portion of the particle suspension ink upon deposition the liquid phase (water labeled with 1%w/v Rhodamine B) diffuses through the 0.5%, 1.5% and 3% xanthan baths resulting in a condensed particle phase, along the nozzle plot trajectory over time. (D) Muscle tissue formation that can be picked up with tweezers. When SMC spheroids are used as particles, they fuse into a homogenous smooth muscle tissue fiber after 7 d of culture, that can be picked up after diluting the xanthan bath to aqueous viscosity concentrations via medium addition.

flow field and the particles do not significantly alter the rheological properties of the liquid [39]. Moving the nozzle horizontally through the xanthan bath results in the formation of a temporary trench, which refills with xanthan momentarily after the passing of the nozzle. When moving a standard straight tip 21G nozzle horizontally through the bath, extruded material tended to flow through the trench along the outside of the nozzle, resulting in a sheet-like formation (figure 2(B (i))). This behavior was not experienced when the standard nozzle was moved vertically through the bath, resulting in a printed vertical line along the path of the nozzle (figure 2(B (ii)), supplementary movie (1). To prevent flow of the ink around the nozzle in the case of horizontal displacement, a 90° bent needle was used (figure 2(B (iii))). By labeling the liquid phase of the ink with a dye, it was shown that the liquid phase diffuses into the xanthan bath after extrusion. This resulted in a straight line of concentrated particle matter along the extrusion path (figure 2(C (i–ii))). To demonstrate the biocompatibility of the approach, SMC spheroids with a diameter of approximately 60 μm at 0.1 ϕ_p were used as the particle fraction of the suspension ink. Printed lines were cultured for 7 d, resulting in a fully fused and compacted tissue fiber (figure 2(D (i–iii))).

3.2. The mechanism of diffusion packing

To further explore the mechanism resulting in the concentration of the printed dilute particle suspensions, a custom imaging set-up was prepared which allowed real time multicolor fluorescent imaging of the multiple components while printing (figures 3 (A) and (B)). Using this set-up, it was confirmed that the extruded material flowed along the outside of the nozzle when a xanthan bath was used (figure 3(C)). To prevent this behavior, the xanthan bath was modified to behave as a Newtonian fluid by adding 2% SA [40]. With this adaptation of the bath, backflow no longer occurred (figure 3(C)). However, while the printing of suspensions within the xanthan–SA bath was still possible, the diffusion packing process no longer occurred but rather the particles mixed with the proximal area of the embedding bath (supplementary figure 1, supplementary movies 2 and 3). This indicates that the shear thinning and self-healing properties of xanthan are crucial for the formation of particle only structures. In order to establish the influence of the ink extrusion rate on the distribution of the ink in the xanthan bath, Coumarin-6 PS particle suspensions at 0.1 ϕ_p in water supplemented with rhodamine B was injected at three different flow rates while keeping the nozzle static (figure 3(D)). At a high flow rate of 2 ml min^{-1}, the liquid jetted and pushed away the xanthan creating an area of turbulence. At an intermediate flow rate of 100 μl min^{-1} the previously observed behavior of backflow along the nozzle was observed. At a low flow rate of 10 μl min^{-1}, the slow entry of suspension in the tip area of the needle was observed (supplementary movie 4). Extrusion at different flow rates was then repeated while simultaneously moving the nozzle (figure 3(D)).

In all cases, the OD of the needle plotted an area where the suspension could enter, and the particles

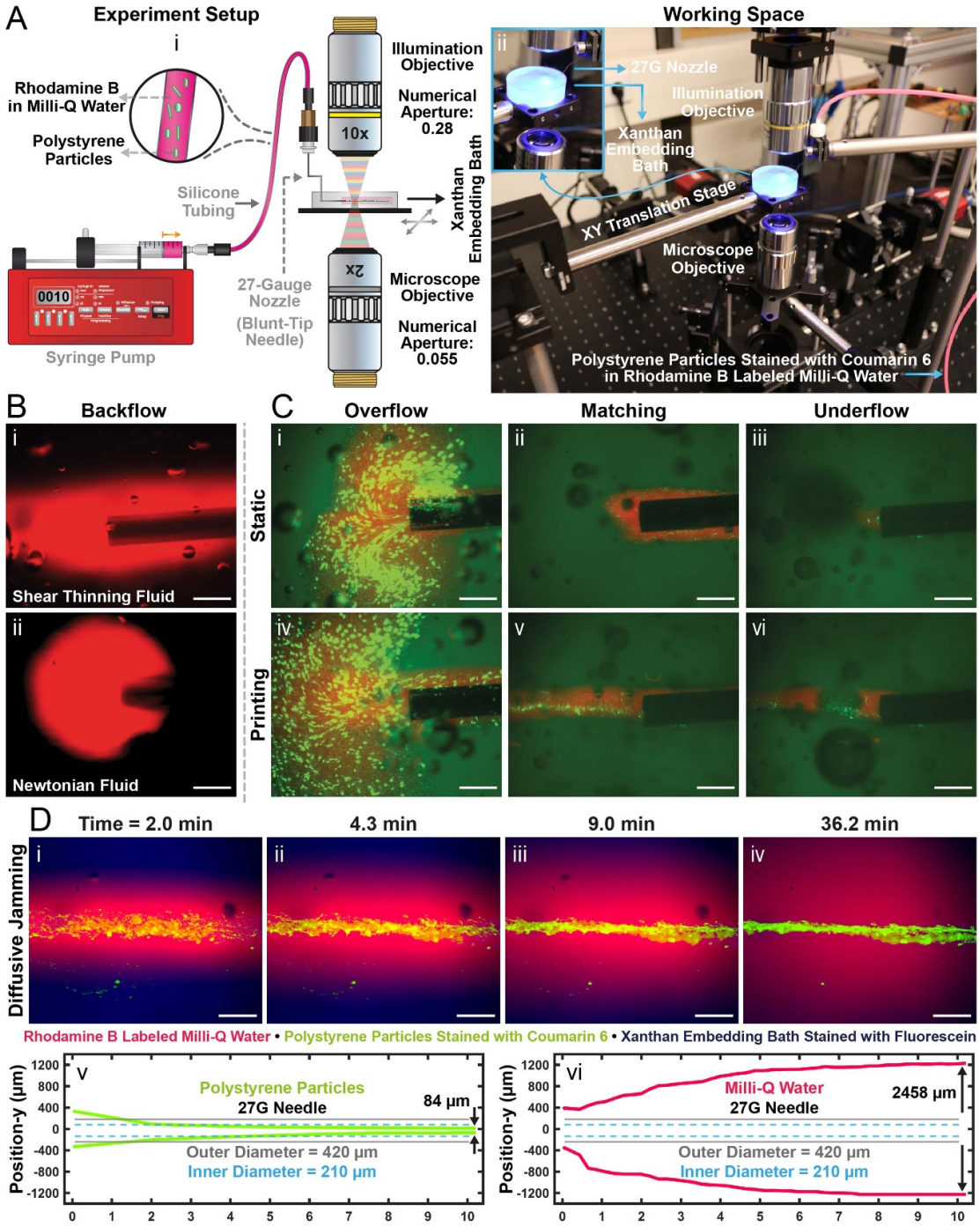

Figure 3. Diffusion packing visualization and analysis. (A) Schematic of experimental setup to visualize in real time the embedded 3D printing of dilute suspension inks and picture of the custom-made imaging setup. (B) Comparison between (i) a shear thinning fluid (1.5% xanthan) and (ii) a Newtonian fluid embedding bath (1.5% xanthan, 2% alginate). In the case of shear thinning fluid, the water labeled with rhodamine B (1 w/v) follows along the nozzle trajectory, while the liquid–liquid interaction of the water and Newtonian fluid bath results in a mixture of the two. (C) Overflow (1 ml min^{-1}), matched flow (100 μl min^{-1}) and underflow (10 μl min^{-1}) of a 10 μl injection volume with a static (i–iii) and moving nozzle (iv–vi) in a 1.5% xanthan bath. In the case of overflow, the liquid violently ruptures the embedding bath, whether it is moving or static. With lower flow rates, the liquid follows the path of least resistance, following the nozzle surface, but when the nozzle is moving while extruding, the suspension fills the cavity opened by the nozzle volume. (D) Diffusion packing imaging over time (i–iv) where diffusion of water labeled with rhodamine B and particle packing is observed simultaneously, and plots of particle position and rhodamine signal over time (v, vi). The final diameter of the feature printed is below nozzle ID, and the initial diameter of the feature is similar to the nozzle's OD. White scale bar = 500 μm.

flowed freely into the plotted area. When the flow rate matched or was below the volume that the needle plotted, backflow was prevented, and the result was a line of particles (figure 3(D (iv))). After extrusion, the particles traveled freely within the area plotted by the OD of the needle. Then a rapid deceleration of the particles was observed, which can be attributed partially to the shear recovery property of the XG

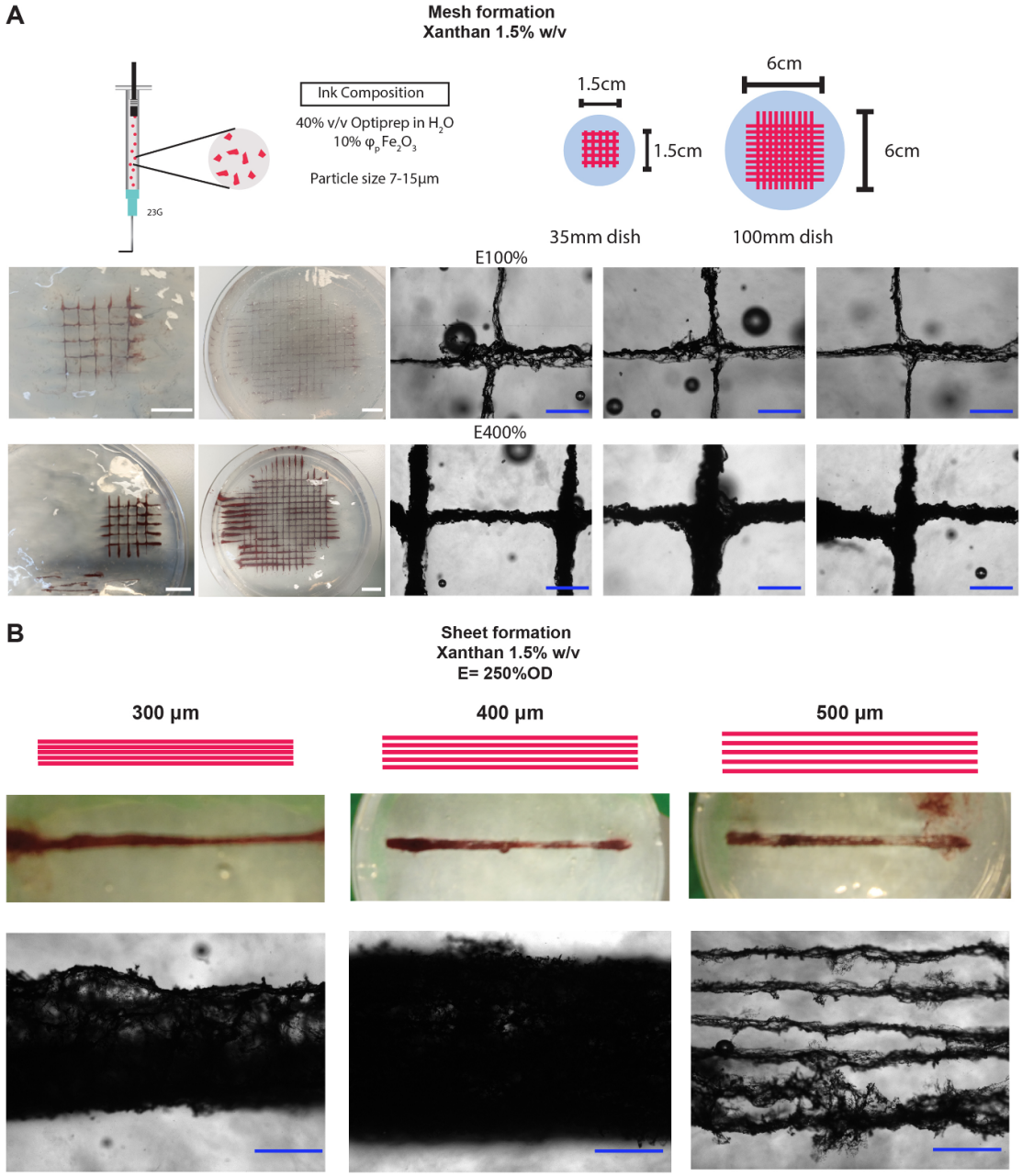

Figure 4. Complex structure printing. (A) Printing of a $\varphi_p = 0.1$ Fe_3O_2 suspension ink in a mesh pattern. There is no difference between different size of meshes (1.5 cm × 1.5 cm vs 6 cm × 6 cm). The Infill rate affects significantly the feature width. (B) Printing of a $\varphi_p = 0.1$ Fe_3O_2 suspension ink into a sheet. For a 23G nozzle, at 250% *E* value based on the OD of the nozzle, the optimal distance for sheet formation is 400 μm. Below that, the structure becomes disrupted, and above 400 μm the linear features start be distinguished. White scale bar = 1 cm blue scale bar: 1 mm.

(supplementary movie 3). A slower process followed, which we named diffusion packing. In this process, the liquid phase of the suspension diffuses into the xanthan matrix, and in tandem the particles converge together until they are in contact, in the center of the plotted area. Over the span of 12 min, the particles came into contact and formed a line feature with a diameter that was drastically lower than the nozzle diameter (figure 3(D (iv))). Particle displacement and water diffusion were quantified by tracing the position of the particles and the rhodamine B signal over time (figure 3(D (v–vi)). A slight tilt could be observed in the diffusion plot, which was in line with the slight angle of the 90° bent needle as seen in figure 3(D (v–vi))). This further demonstrated that the area of inflow is determined by the nozzle architecture. The line diameter after diffusion jamming was 84 μm when using a 27G nozzle (ID ∼ 210 μm), showing that a resolution significantly lower than the nozzle diameter can be achieved.

3.3. Printing of features

To demonstrate the 3D printing of features other than straight lines, both a small and a large mesh pattern

were printed using an ink containing 0.1 ϕ_p Fe_2O_3 particles (figure 4(A), supplementary movie 7). The results show that features were printed reproducibly and that the disturbances caused by intersecting lines were minimal. Additionally, an approach to print sheets was explored by printing series of subsequent lines with varying interline distances (figure 4(B)). This showed that for a 23G nozzle and an infill rate of 250%, a reproducible sheet could be formed when a distance of 400 μm between the center of subsequent lines was used. A lower distance of 300 μm resulted in an excessive accumulation of particles and with that an irregular sheet, while a higher distance of 500 μm resulted in gaps between the subsequent lines after the diffusion packing process.

3.4. Platform potential

For all inks investigated in this study, the particles of the suspension inks initially flowed freely into the nozzle plot region, then through diffusion packing they concentrated and came into contact forming dense particle lines. Alginate particles and collagen particle lines were stable over time (supplementary figure 2). CMs, IPSCs and SMC spheroids fused over time forming micro-tissues (figures 5(B)–(D)). The morphology of these tissues varied based on the fusion potential of the cells or cell spheroids used. Specifically the SMC spheroids formed a rigid fiber that could be picked up with tweezers (figure 2(C), supplementary figure 3), a feature that was also observed for other formulations including iPSCs, and SMCs in combination with PLA particles. In the absence of cells, the particles stay in place (supplementary figure 2). When testing combinations of collagen-coated particles with SMC cells and SMC spheroids respectively, self-assembly of a composite tissue was observed over time. Due to tissue compaction, the line feature transformed into multiple tissue globules, centered around the areas with the highest initial cell and spheroid concentration (figures 5(E) and (F)). Regions of interest were imaged using Z-stacking to observe the tissue architecture. This showed that the cellular matter surrounded the particles, and integrated them into a composite tissue.

In all investigated cases, the mean diameter of the printed fibers was below the nozzle ID, as previously observed in the diffusion packing experiments. In order to tune the diameter of a feature, the amount of extruded material was varied, by varying the infill rate, commonly marked as E value in the g-code of a printer. A direct analogous correlation could be observed between infill rate and resulting fiber diameter (figure 5(A)). However there is an upper limit to this, since over exceeding the injected volume leads to backflow of the suspension towards the nozzle or jetting as shown in (figure 3(D)). An infill rate scan using an ink consisting of 0.10 ϕ_p iron oxide particles showed that backflow starts at an infill rate of 250% and the structure bursts at an infill rate of 750% (supplementary figure 4). Thus a direct correlation between the amount of particles and feature diameter could be deducted, with an observed minimum limit, since simply using too few particles, might result in a centered, but uneven line (supplementary figure 2). In order to compare our approach with conventional parameters that affect printing resolution, the use of different printing nozzles was also tested. This showed that using a smaller nozzle only has a marginal effect on the average feature resolution of the lines (figure 5(A)). However, the consistency of the line width was improved along its length.

3.5. Self-assembly of fiber organoids

While in section 3.4, we already observed the fusion of cellular matter into fibers, which can be considered a self-assembly process, we hypothesized that the fibers could further remodel over time. To test this, we 3D printed lines of hPSC-derived CMs and hPSC-derived epicardial cells which both express different fluorescent proteins to allow for tracking of the two cell types [41]. The hPSC-CMs express GFP from the NKX2.5 genomic locus and have an alpha-actinin-mRubyII fusion protein. NKX2.5 is a cardiac marker present in cardiac progenitors and contracting CMs and alpha-actinin is a sarcomeric protein of the contractile machinery in CMs (figure 6(A)). The hPSC-epicardial cells in the printed constructs can be identified by endogenous expression of red fluorescent mCherry from the COUP-TFII locus. COUP-TFII is expressed in epicardial cells but is absent from ventricular CMs (figure 6(A)). In figure 6(B), it can be observed that the cardiac/epicardial cell constructs compacted to a connected fiber within 3 d. After day 3, fibers elongated until day 8, after which the fibers shortened. At locations where the cell density is too low, the fiber segregated into smaller cell spheroids (supplementary figure 5). As shown in figure 6(C), based on the fluorescent distribution within the cell construct on day 0, the cells were randomly dispersed immediately after printing. Over time, the cells gradually migrated within the fiber construct to form a two-layered tissue within the time course of 13 d consisting of a body of CMs covered by a layer of epicardial cells, which resembles the organization seen in human heart tissue. At day 13, confocal microscopy was performed to examine sarcomere formation and the homogenous distribution of alpha-actinin within the fiber tissue was observed (figure 6(D)). Spontaneous beating was observed on day 8. After electrical pacing of the cardiac fibers, tissues started beating

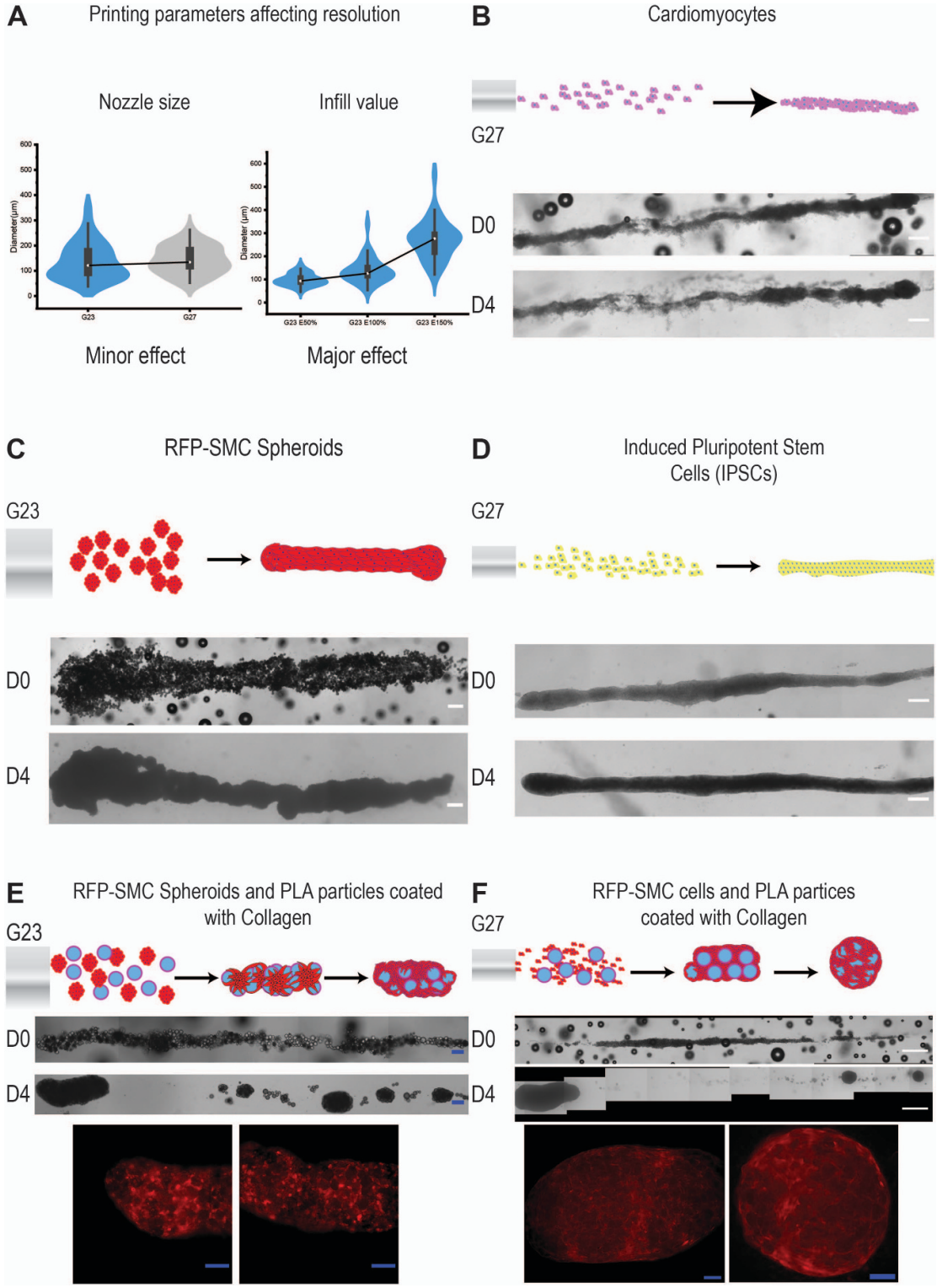

Figure 5. (A) Printing resolution dependency on nozzle size and infill percentage. Changing the nozzle size has a minor effect on print resolution (B) printing of CMs, (C) printing of SMC spheroids, (D) printing of IPSCs, (E) printing of SMCs spheroids with collagen-coated particles, (F) printing of SMC cells with collagen- coated particles. In all cases, line formation can be observed, but over cell culture duration, self-assembly into tissue fibers or particle-cell tissue composites are observed. The tissue thickness post-deposition differs between CMs which have a low proliferation rate, and IPSCs that have a high proliferation rate. White scale bar = 500 μm, blue scale bar = 100 μm.

synchronously and could follow a pacing frequency up to 4 Hz (figures 6(E) and (F), supplementary movie 8). When the fibers were brought into contact with the plate surface that allowed adhesion, spontaneous attachment of the tissue fiber was observed (figure 6(G)).

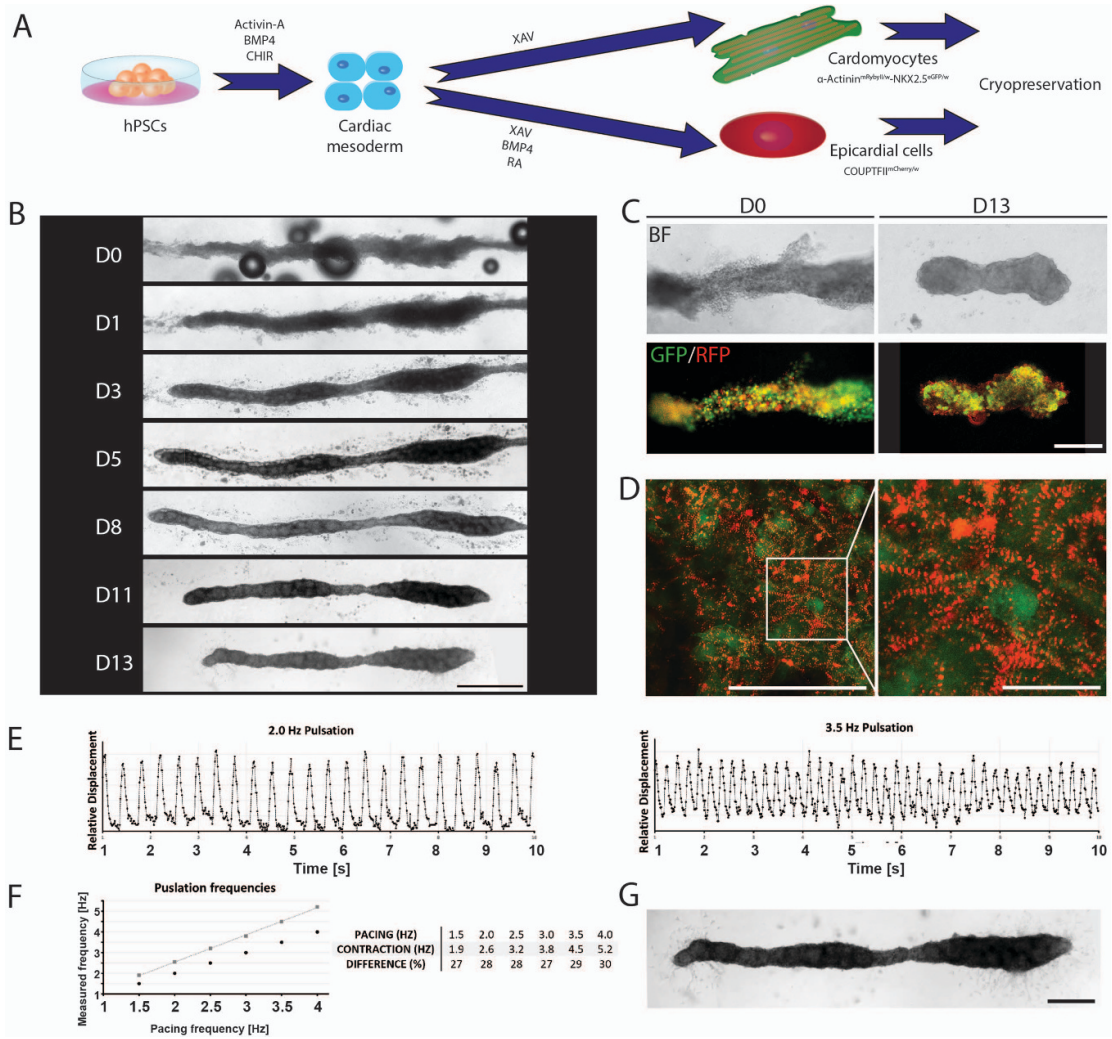

Figure 6. Bioprinting of cardiac tissues. (A) Schematic of the cardiac differentiation towards contracting CMs and epicardial cells with endogenous expression of specific fluorescent reporters. (B) Time-course of tissue formation after printing (scale bar = 1000 μm). (C) Brightfield and fluorescent images of a printed fiber at day 0 and 13 after bioprinting to show the migratory property of the cells within the fiber resulting in a layer of ECCs covering the CMs (scale bar = 250 μm). (D) Fluorescent images of the mRubyII-ACTN2 and GFP-NKX2.5 (DRRAGN) reporter to visualize sarcomere formation in fibers (scale bar = 100 μm (left panel) and 25 μm (right panel)), (E) line graph of the electrical pacing at 2.0 and 3.5 Hz, (F) correlation graph of the electrical pacing frequency with actual contraction frequency from 1.5 till 4 Hz and (G) cardiac fiber tissue with filopodia connected to the surface of the culture dish (scale bar = 1000 μm).

4. Discussion

In this work, we present a strategy to 3D print dilute suspensions of particles that can self-assemble into tissue and hybrid tissue fibers. Our main objective was to find a way to print cellular matter in a way that mimics standard cell culture procedures, avoiding material addition for the purpose of rheological modification. While low viscosity inks present somewhat those advantages, using aqueous suspensions is the ideal scenario for mimicking cell culture practices. To the best of our knowledge, we are the first to observe and utilize the phenomenon of diffusion packing for the purpose of printing, even though we suspect that it is present in most of the embedded printing work when it comes to printing within yield stress fluids. XG is a highly utilized and inexpensive material of the food industry, and using it with the cost-effective 3D printing technique of extrusion makes this methodology accessible to most labs that can perform cell culture. While xanthan hydrogels have been demonstrated as useful embedding baths of bulk hydrogel inks, the behavior of diffusion packing is not present as shown in previous work [30] and our own experiments.

The main challenge was imaging the diffusion packing process, since it is an interaction between multiple matter states, namely suspensions that behave like liquids, particles flowing and the liquid portion of the suspension diffusing into the xanthan matrix, and the yield stress fluid behavior of xanthan under dynamic conditions. Through real-time imaging, we were able to break down the components of this process. Using this process, at the moment we can reproducibly fabricate fibers and a mesh pattern, as well as sheets which are composed of overlapping

printed lines (figure 4). Current work is focusing on an alternative method for the printing of sheets based on a repetitive sideways motion of the nozzle, where we already have indications that this is possible as long as the area opened by the needle does not collapse before the ink is extruded (supplementary movie 5).

We compared embedding baths with Newtonian fluid behavior and aqueous viscosity (XG 1.5% alginate 2%) and yield stress fluid behavior (XG 0.5%–3%) [40, 42]. While Newtonian fluid behavior embedding baths allowed complex 3D printing similar to previously published work [14], the embedding bath phase mixed with the feature regime leading to a mixture of both the bath and the ink (supplementary movie 2) which interferes with the self-assembly process of cells. Therefore we focused on the yield stress fluid embedding bath formulation (1.5% XG) since we observed no mixing of the bath with the ink deposition area. We suspect that in previously published works that included embedded particle suspensions [15–17, 29] diffusion packing likely occurred. However, the embedding baths may have been tuned to be more liquid-like similar to (figure 3(C)). In these works, the embedding bath interacts with the tissue, meaning that the bath has to be optimized to be biocompatible. Xanthan on the other hand, is bioinert chemotactically. This assisted in observing the self-assembly behavior of our tissues without the interaction with biomaterials. We further showed that xanthan can also be printed into a spatially patterned embedding bath (supplementary movie 6 and supplementary figure 6). As xanthan can be chemically modified to enable specific interactions with the developing tissue [43, 44], patterned embedding baths offer the potential to locally affect tissue development.

Our approach removes the prerequisites of shear thinning and shear recovery properties of the ink, thus enabling the printing of cellular matter, and any biomaterial that can be in a particle suspension without significant particle-particle interactions. In order to avoid jamming events, we maintain a 5.14× nozzle to particle diameter ratio [45]. In most cases of extrusion 3D printing, the feature resolution is determined by the nozzle diameter. The resolution of features in our work was smaller than the nozzle diameter due to the process of diffusion packing. The key parameter of our approach is the influx of particles, which is determined by the φ_p of the suspension and the extruded volume. Higher volume fractions dispensed, lead to more particles being in the print area, which leads to thicker features.

Another element of the platform is that the composition of the suspension ink can be tuned to contain combinations of cells and particles. In both cases of SMC spheroids with collagen-coated PLA particles and SMC cells with collagen coated-particles, we observed a self-assembly process into a composite porous tissue. The tissue composite that formed through this self-assembly process presented no necrosis in its center, as nutrients can be supplied via the cavities formed by the collagen beads, similar to the work of Matsunaga *et al* where molded composite micro-tissues formed structures of several mm [46]. Furthermore, hydrogel beads that have cells encapsulated within them can also be incorporated into the ink suspension in order to add another degree of tissue complexity [47]. Microfluidic breakthroughs have allowed the production of tailored hydrogel beads that can contain cells, release growth factors, have Janus interfaces, and have a modified surface that can interact on demand with the cells [36, 48, 49]. Moreover, at any given point during culture, a nozzle can be re-inserted into the bath in order to provide a time-specific cue to the cells, as long as the bath is not significantly diluted. This allows stimulation on demand, whether it is the addition of a new growth factor, a new print or electrostimulation. The potential toolbox of combinations, where each type of particle included can allow or prevent adhesion, or elute a different growth factor, has the potential to combine organoid drug testing with microfluidic particle advances, into an accessible 3D printing platform.

Using the diffusion packing approach, we demonstrated the self-assembly of a dense self-assembled beating cardiac fiber. We observed that the two cell types, hPSC-derived CMs and hPSC-derived epicardial cells, actively migrated within the fibers to form a bi-layered cardiac tissue with contracting CMs in the middle part surrounded by a protective layer of epicardial cells, which is similar to the middle and outer layer in the *in vivo* heart. We believe that this natural self-assembly process is facilitated by the absence of a hydrogel matrix, which would increase the distance between the cells and affect the self-assembly process. Cardiac fibers formed a homogenous distribution of sarcomeres within the tissues and started to contract spontaneously. However, the sarcomeres were randomly orientated and did not align, which is most likely due to the lack of mechanical anchoring of the tissue. After electrical stimulation, bioprinted fibers followed a pacing frequency up to 4 Hz. Nevertheless, we noted a discrepancy of about 30% between the pacing and actual frequency. This might be related to the difficulty in measuring the actual pacing frequency because the fibers are embedded in xanthan, and not attached to a surface.

5. Conclusions

Our approach allows the simple and inexpensive 3D printing of dilute particle suspensions, into self-assembled, dense, complex tissue fibers. Since the need for a hydrogel phase was bypassed, the cells and spheroids readily fuse and organize into functioning structures, as shown in the beating cardiac fiber print.

Moreover, there is an abundance of potential customization, since the xanthan bath can be 3D printed with defined compartments, to stimulate the subsequently printed tissue in a spatially defined pattern. Furthermore, chemotactic cues can be introduced via simple liquid addition on top of the bath since the permeability of the bath allows liquid diffusion. Mechanical and electrical stimulation is also possible during culture, as demonstrated by the pacing of the cardiac fiber. Finally, this approach is inexpensive and can be readily adapted to any extrusion bioprinter.

Data availability statement

The data that support the findings of this study are available upon reasonable request from the authors.

Acknowledgment

We thank Dr Claas Willem Visser for his feedback during the preparation of this study.

Funding

This project was funded by the European Research Council (ERC) under the European Union's Horizon 2020 Research and Innovation Programme (No. 724469 and No. 638428).

Ethical statements

This research does not include human participants or animal materials. Human cell cultures have been performed in accordance with the approved workflow at the University of Twente.

ORCID iDs

Vasileios D Trikalitis https://orcid.org/0000-0001-8309-0010
Mert Kaya https://orcid.org/0000-0002-7123-7334
Carla Cofiño-Fabres https://orcid.org/0000-0002-3947-1294
Simone ten Den https://orcid.org/0000-0001-5727-182X
Islam S M Khalil https://orcid.org/0000-0003-0617-088X
Sarthak Misra https://orcid.org/0000-0003-4961-0144
Bart F J M Koopman https://orcid.org/0000-0001-5091-1724
Robert Passier https://orcid.org/0000-0003-4312-9296
Verena Schwach https://orcid.org/0000-0003-1831-7412
Jeroen Rouwkema https://orcid.org/0000-0001-9666-9064

References

[1] Shapira A and Dvir T 2021 3D tissue and organ printing—hope and reality *Adv. Sci.* **8** 2003751
[2] Dey M and Ozbolat I T 2020 3D bioprinting of cells, tissues and organs *Sci.Rep.* **10** 14023
[3] Shahbazi M N *et al* 2016 Self-organization of the human embryo in the absence of maternal tissues *Nat. Cell Biol.* **18** 700–8
[4] Hofer M and Lutolf M P 2021 Engineering organoids *Nat. Rev. Mater.* **6** 402–20
[5] Ozbolat I T, Peng W and Ozbolat V 2016 Application areas of 3D bioprinting *Drug Discov. Today* **21** 1257–71
[6] Ovsianikov A, Khademhosseini A and Mironov V 2018 The synergy of scaffold-based and scaffold-free tissue engineering strategies *Trends Biotechnol.* **36** 348–57
[7] Jiang T, Munguia-Lopez J G, Flores-Torres S, Kort-Mascort J and Kinsella J M 2019 Extrusion bioprinting of soft materials: an emerging technique for biological model fabrication *Appl. Phys. Rev.* **6** 011310
[8] Cooke M E and Rosenzweig D H 2021 The rheology of direct and suspended extrusion bioprinting *APL Bioeng.* **5** 011502
[9] Pössl A *et al* 2021 A targeted rheological bioink development guideline and its systematic correlation with printing behavior *Biofabrication* **13** 035021
[10] Da Silva K, Kumar P, Choonara Y E, du Toit L C and Pillay V 2020 Three-dimensional printing of extracellular matrix (ECM)-mimicking scaffolds: a critical review of the current ECM materials *J. Biomed. Mater. Res. A* **108** 2324–50
[11] Morley C D *et al* 2019 Quantitative characterization of 3D bioprinted structural elements under cell generated forces *Nat. Commun.* **10** 3029
[12] Lewis-Israeli Y R *et al* 2021 Self-assembling human heart organoids for the modeling of cardiac development and congenital heart disease *Nat. Commun.* **12** 5142
[13] Green J B A and Sharpe J 2015 Positional information and reaction-diffusion: two big ideas in developmental biology combine *Development* **142** 1203–11
[14] Kajtez J *et al* 2022 Embedded 3D printing in self-healing annealable composites for precise patterning of functionally mature human neural constructs *Adv. Sci.* **9** 2201392
[15] Bhattacharjee T *et al* 2016 Liquid-like solids support cells in 3D *ACS Biomater. Sci. Eng.* **2** 1787–95
[16] Jeon O, Lee Y B, Jeong H, Lee S J, Wells D and Alsberg E 2019 Individual cell-only bioink and photocurable supporting medium for 3D printing and generation of engineered tissues with complex geometries *Mater. Horiz.* **6** 1625–31
[17] Brassard J A, Nikolaev M, Hübscher T, Hofer M and Lutolf M P 2021 Recapitulating macro-scale tissue self-organization through organoid bioprinting *Nat. Mater.* **20** 22–29
[18] Iordan A, Duperray A and Verdier C 2008 Fractal approach to the rheology of concentrated cell suspensions *Phys. Rev.* E **77** 011911
[19] Nair K, Gandhi M, Khalil S, Yan K C, Marcolongo M, Barbee K and Sun W 2009 Characterization of cell viability during bioprinting processes *Biotechnol. J.* **4** 1168–77
[20] Cidonio G, Glinka M, Dawson J I and Oreffo R O C 2019 The cell in the ink: improving biofabrication by printing stem cells for skeletal regenerative medicine *Biomaterials* **209** 10–24
[21] Toh Y C and Voldman J 2011 Fluid shear stress primes mouse embryonic stem cells for differentiation in a self-renewing environment via heparan sulfate proteoglycans transduction *FASEB J.* **25** 1208–17
[22] Huang Y, Chen X, Che J, Zhan Q, Ji J and Fan Y 2019 Shear stress promotes arterial endothelium-oriented differentiation of mouse-induced pluripotent stem cells *Stem Cells Int.* **2019** 1847098
[23] Gratson G M, Xu M and Lewis J A 2004 Direct writing of three-dimensional webs *Nature* **428** 386

[24] Bhattacharjee T, Zehnder S M, Rowe K G, Jain S, Nixon R M, Sawyer W G and Angelini T E 2015 Writing in the granular gel medium *Sci. Adv.* **1** 1500655
[25] Shiwarski D J, Hudson A R, Tashman J W and Feinberg A W 2021 Emergence of FRESH 3D printing as a platform for advanced tissue biofabrication *APL Bioeng.* **5** 010904
[26] Daly A C, Davidson M D and Burdick J A 2021 3D bioprinting of high cell-density heterogeneous tissue models through spheroid fusion within self-healing hydrogels *Nat. Commun.* **12** 753
[27] Skylar-Scott M A, Uzel S G M, Nam L L, Ahrens J H, Truby R L, Damaraju S and Lewis J A 2019 Biomanufacturing of organ-specific tissues with high cellular density and embedded vascular channels *Sci. Adv.* **5** eaaw2459
[28] Kumar A, Rao K M and Han S S 2018 Application of xanthan gum as polysaccharide in tissue engineering: a review *Carbohydr. Polym.* **180** 128–44
[29] Noor N, Shapira A, Edri R, Gal I, Wertheim L and Dvir T 2019 3D Printing of Personalized Thick and Perfusable Cardiac Patches and Hearts *Adv. Sci.* **6** 1900344
[30] Patrício S G, Sousa L R, Correia T R, Gaspar V M, Pires L S, Luís J L, Oliveira J M and Mano J F 2020 Freeform 3D printing using a continuous viscoelastic supporting matrix *Biofabrication* **12** 035017
[31] Nelson A Z, Kundukad B, Wong W K, Khan S A and Doyle P S 2020 Embedded droplet printing in yield-stress fluids *Proc. Natl. Acad. Sci.* **117** 5671–9
[32] Daly A C, Riley L, Segura T and Burdick J A 2019 Hydrogel microparticles for biomedical applications *Nat. Rev. Mater.* **5** 20–43
[33] Schwach V, Verkerk A O, Mol M, Monshouwer-Kloots J J, Devalla H D, Orlova V V, Anastassiadis K, Mummery C L, Davis R P and Passier R 2017 A COUP-TFII human embryonic stem cell reporter line to identify and select atrial cardiomyocytes *Stem Cell Rep.* **9** 1765–79
[34] Birket Matthew J *et al* 2015 Contractile defect caused by mutation in MYBPC3 revealed under conditions optimized for human PSC-cardiomyocyte function *Cell Rep.* **13** 733–45
[35] Ng E S, Davis R, Stanley E G and Elefanty A G 2008 A protocol describing the use of a recombinant protein-based, animal product-free medium (APEL) for human embryonic stem cell differentiation as spin embryoid bodies *Nat. Protocols* **3** 768
[36] Kamperman T, Trikalitis V D, Karperien M, Visser C W and Leijten J 2018 Ultrahigh-throughput production of monodisperse and multifunctional janus microparticles using in-air microfluidics *ACS Appl. Mater. Interfaces* **10** 23433–8
[37] Kaya M, Stein F, Padmanaban P, Zhang Z, Rouwkema J, Khalil I S and Misra S 2022 Visualization of micro-agents and surroundings by real-time multicolor fluorescence microscopy *Sci Rep.* **12** 13375
[38] Kaya M, Stein F, Rouwkema J, Khalil I S M and Misra S 2021 Serial imaging of micro-agents and cancer cell spheroids in a microfluidic channel using multicolor fluorescence microscopy *PLOS ONE* e0253222
[39] Batchelor G K and Green J T 1972 The Hydrodynamic Interaction of Two Small Freely-Moving Spheres in a Linear Flow Field *J. Fluid Mech.* **56** 375–400
[40] Pongjanyakul T and Puttipipatkhachorn S 2007 Xanthan-alginate composite gel beads: molecular interaction and *in vitro* characterization *Int. J. Pharm.* **331** 61–71
[41] Ribeiro M C, Slaats R H, Schwach V, Rivera-Arbelaez J M, Tertoolen L G J, van Meer B J, Molenaar R, Mummery C L, Claessens M M A E and Passier R 2020 A cardiomyocyte show of force: a fluorescent alpha-actinin reporter line sheds light on human cardiomyocyte contractility versus substrate stiffness *J. Mol. Cellular Cardiol.* **141** 54
[42] Gruber J V and Konish P N 1999 Building Aqueous Viscosity through Synergistic Polymer-Polymer Interactions *Polysaccharide Applications* (Oxford : Oxford University Press) pp 252–61
[43] Glaser T, Bueno V B, Cornejo D R, Petri D F S and Ulrich H 2015 Neuronal adhesion, proliferation and differentiation of embryonic stem cells on hybrid scaffolds made of xanthan and magnetite nanoparticles *Biomed. Mater.* **10** 045002
[44] Alavarse A C, Frachini E C G, Silva J B, D Spereira R, Ulrich H and Petri D F S 2022 Amino acid decorated xanthan gum coatings: molecular arrangement and cell adhesion *Carbohydrate Polymer Technologies and Applications* **4** 100227
[45] Souzy M, Zuriguel I and Marin A 2020 Transition from clogging to continuous flow in constricted particle suspensions *Phys. Rev.* E **101** 060901
[46] Matsunaga Y T, Morimoto Y and Takeuchi S 2011 Molding cell beads for rapid construction of macroscopic 3D tissue architecture *Adv. Mater.* **23** H90–4
[47] Visser C W, Kamperman T, Karbaat L P, Lohse D and Karperien M 2018 In-Air microfluidics enables rapid fabrication of emulsions, suspensions, and 3D modular (Bio)materials *Sci. Adv.* **4** eaao1175
[48] Gu F, Amsden B and Neufeld R 2004 Sustained delivery of vascular endothelial growth factor with alginate beads *J. Control. Release* **96** 463–72
[49] Feng Q, Li D, Li Q, Cao X and Dong H 2022 Microgel assembly: fabrication, characteristics and application in tissue engineering and regenerative medicine *Bioact. Mater.* **9** 105–19